Acta Materialia 245 (2023) 118585

Contents lists available at ScienceDirect

Acta Materialia

journal homepage: www.elsevier.com/locate/actamat

Tensile overload-induced texture effects on the fatigue resistance of a CoCrFeMnNi high-entropy alloy

Tu-Ngoc Lam [a,b], Hsu-Huan Chin [a], Xiaodan Zhang [c], Rui Feng [d], Huamiao Wang [c], Ching-Yu Chiang [e], Soo Yeol Lee [f,*], Takuro Kawasaki [g], Stefanus Harjo [g], Peter K. Liaw [d], An-Chou Yeh [h,i], Tsai-Fu Chung [a], E-Wen Huang [a,i,**]

[a] Department of Materials Science and Engineering, National Yang Ming Chiao Tung University, Hsinchu 30010, Taiwan
[b] Department of Physics, College of Education, Can Tho University, Can Tho 900000, Viet Nam
[c] State Key Laboratory of Mechanical System and Vibration, Shanghai Jiao Tong University, Shanghai 200240, China
[d] Department of Materials Science and Engineering, The University of Tennessee, Knoxville, TN 37996, USA
[e] National Synchrotron Radiation Research Center, Hsinchu 30076, Taiwan
[f] Department of Materials Science and Engineering, Chungnam National University, Daejeon 34134, Republic of Korea
[g] J-PARC Center, Japan Atomic Energy Agency, 2-4 Shirane Shirakata, Tokai-mura, Naka-gun, Ibaraki 319-1195, Japan
[h] Department of Materials Science and Engineering, National Tsing Hua University, Hsinchu 30013, Taiwan
[i] High Entropy Materials Center, National Tsing Hua University, Hsinchu 30013, Taiwan

ARTICLE INFO

Keywords:
High-entropy alloy
Fatigue-crack propagation
Tensile overload
Retardation
Texture

ABSTRACT

The present study investigates the crystallographic-texture effects on the improved fatigue resistance in the CoCrFeMnNi high-entropy alloys (HEAs) with the full-size geometry of the American Society for Testing and Materials (ASTM) Standards E647-99. We exploited X-ray nano-diffraction (XND) mapping to characterize the crystal-deformation levels ahead of the crack tip after stress unloading under both constant- and tensile-overloaded-fatigue conditions. The crack-tip blunting-induced much higher deformation level was concentrated surrounding the crack-tip which delays the fatigue-crack growth immediately after a tensile overload. The predominant deformation texture orientation in the Paris regime was investigated, using electron backscatter diffraction (EBSD) and orientation distribution function (ODF) analyses. The twinning formation-driven shear deformation gave rise to the development of the Goss-type texture within the plastic deformation regime under a tensile-overloaded-fatigue condition, which was attributed to enhance the crack deflection and thus the tensile-induced crack-growth-retardation period in the CoCrFeMnNi HEA. Our new findings address the quantitative discrepancy found in our earlier work.

1. Introduction

Fatigue limit is one of the most important factors in determining the lifetime of structural materials since they often experience various cyclic-loading conditions. Improving the resistance to fatigue-crack propagation (FCP) is one of the most decisive criteria for practical engineering applications of materials [1–3]. From the viewpoint of grain crystallography, the fatigue-crack path is regulated by the grain size, grain boundary, and slip band since the crack propagates along the grain boundaries or through the grains via an activated slip band upon cyclic loading. There have been great efforts to clarify their mutual relation on the FCP resistance. Kunkler *et al.* proposed a two-dimensional model of texture effects on the crack-growth behavior in the transition from fatigue stages I to II [4]. Zhao et al. reported a pivotal role of Goss, P, and Q textures in the Paris regime (stage II) and a beneficial role of a balanced crack deflection-crack closure to great FCP resistance in aluminum alloys [3]. Liu et al. observed the retardation of FCP in stage II by Goss-oriented grains in aluminum alloys [5].

One of the most effective ways to induce the crack-growth-retardation behavior in the Paris regime is applying a much higher single tensile overload [6–12]. Among the widely explored alloys, high-entropy alloys (HEAs) [13] have emerged as the potential

* Corresponding author.
** Corresponding author at: Department of Materials Science and Engineering, National Yang Ming Chiao Tung University, Hsinchu 30010, Taiwan.
E-mail addresses: sylee2012@cnu.ac.kr (S.Y. Lee), EwenHUANG@nctu.edu.tw (E.-W. Huang).

https://doi.org/10.1016/j.actamat.2022.118585
Received 13 September 2022; Received in revised form 25 November 2022; Accepted 1 December 2022
Available online 2 December 2022

structural materials with superior mechanical and fatigue properties of the well-balanced strength-ductility and good fatigue resistance, respectively, accompanied with high thermal stability [14–24]. Comprehensive studies on fatigue-crack-growth behavior in the HEAs have been devoted to understanding the relation among processing parameters, structures, and fatigue performance [2,10,15,16,25–28]. Our previous study demonstrated the enhanced fatigue resistance in the single-phase face-centered-cubic (fcc) CoCrFeMnNi HEA by immediately applying a single tensile overload [10]. Possible mechanisms were reported in which the combined effects of the large plastic deformation and predominant twin structures were proposed to delay the fatigue-crack growth in the Paris regime in the CoCrFeMnNi HEA [10].

The distinct microstructure and texture components are responsible for different deformation and fatigue behaviors. Recent attempts have been focused on clarifying the evolution of microstructures and crystallographic orientations of grains during different processing and annealing conditions in the HEAs [29–31]. However, understanding the deformation-texture orientation-dominated fatigue-crack growth in the HEAs upon cyclic loading has not been acquired yet. A transition of microstructural defects from the planar dislocation slip to twin structures was found immediately after a single tensile overload in the CoCrFeMnNi HEA [10] with the qualitative agreement. Moreover, it is of great interest to elucidate how the deformation texture develops and its effects immediately after a single tensile overload, which influence the crack-growth retardation behavior simultaneously.

To gain a more complete viewpoint of immediately applied single tensile overload-induced improved FCP resistance in the CoCrFeMnNi HEA [10], we extend our previous work towards the variance of single tensile-overload-driven crystallographic-texture components in the Paris regime. In this study, we perform the investigation with the full-size geometry of the American Society for Testing and Materials (ASTM) Standards E647-99 in terms of the crystallographic texture effects [32]. The distributions of different crystallographic planes as a function of the distance from the crack tip after stress unloading under both constant- and tensile-overloaded-fatigue conditions were explored via neutron-diffraction measurements. The crystal-deformation level around the crack tip was identified via X-ray nano-diffraction (XND) mapping. The effects of deformation-texture components on the tensile overload-induced crack-growth retardation period were characterized by the electron backscatter diffraction (EBSD) and orientation distribution function (ODF) analyses. Furthermore, the micromechanical deformation behavior of the CoCrFeMnNi under a tensile-overloaded-fatigue condition was understood, using crystal plasticity finite element method (CPEEM).

2. Experimental details

2.1. Sample preparation

The as-cast CoCrFeMnNi HEAs were prepared via vacuum induction melting (VIM) of the alloying elements with purities more than 99.9% (in weight percent).

The compact-tension (CT) CoCrFeMnNi HEAs have a width and thickness of 50.8 and 6.35 mm, respectively, following the ASTM Standards E647-99 for the fatigue test [32]. Before the FCP test, the CT specimens were pre-cracked to an initial crack length of 1.27 mm. The as-fatigued specimen was prepared under constant-amplitude cyclic loading ($P_{max} = 7400$ N and $P_{min} = 740$ N) while the overloaded sample was conducted with the addition of a single tensile overload (10,360 N) at the crack length of 16 mm. More details of the geometry of CT specimens and the two fatigue conditions of as-fatigued and overloaded samples can be referred in our previous study [10].

2.2. Neutron-diffraction measurement

Neutron-diffraction measurements were carried out at the TAKUMI beamline in Materials and Life Science Experimental Facilities at the Japan Proton Accelerator Research Complex (J-PARC), Japan. At the TAKUMI, two orthogonal strain components can be measured simultaneously from the two detector banks situated at $\pm 90^{\circ}$ from an incident neutron beam. Through rotating the CT samples by 90^{o}, we determined all of the three orthogonal strain components namely, the crack-growth direction (or a longitudinal direction, LD), crack-opening direction (or a transverse direction, TD), and through-thickness direction (or a normal direction, ND) of the CT specimen. We performed neutron-strain mapping along the LD direction, which allowed to examine the residual-strain distributions as a function of the distance from the crack tip. A schematic illustration of neutron-diffraction measurements around the crack tip of a CT specimen and the neutron-diffraction geometry for the three-orthogonal strain mapping was presented in Fig. 1.

2.3. Microstructural characterization

The specimens used for microstructural characterization were cut in the vicinity of the crack tip of the CT sample after stress unloading under both constant- and tensile-overloaded-fatigue conditions. The sample surfaces were mechanically polished, using silicon-carbide sandpapers of 4000-grit with a non-crystallizing colloidal silica suspension, and were finally electro-polished. The dendrite structures of as-cast CoCrFeMnNi HEAs were identified, using a polarized optical microscope (POM). The EBSD analysis for grain orientation was performed, employing scanning electron microscopy (SEM, JEOL JSM-7800F NordlysMax3) operated at 20 keV.

The deformation texture was examined via ODF analysis. The ODF charts as a function of the distance from the crack tip were analyzed from the corresponding EBSD orientation mapping as a function of the distance from the crack tip. The ODF evolution was calculated, using the Matlab open toolbox MTEX package [33].

2.4. X-ray fluorescence and X-ray nanodiffraction

X-ray fluorescence (XRF) and XND maps were conducted at the Taiwan Photon Source (TPS) 21A beamline, National Synchrotron Radiation Research Center (NSRRC), Taiwan. The beam energy of 8 keV in XRF maps was used to excite all the constituent elements with a high spatial resolution of 90 nm and a step size of 10 μm. The XND map was exploited with a step size of 10 μm to investigate the full width area (FW) of Laue diffraction caused by surface defects [34]. The evolution of FW represents the cyclic loading-induced crystal deformation level in the vicinity of the fatigue-crack tip.

2.5. Crystal plasticity finite element method

The micromechanical behaviors of the CT CoCrFeMnNi following the ASTM Standards E647-99 model under fatigue tests were simulated, using the finite element code, ABAQUS [35], with a user material model that was programmed based on the crystal plasticity theory. Deformation by dislocation slip/twinning on active slip/twinning systems and the rotation of the crystal lattice under finite deformation have been considered in a constitutive model [36–44]. The constitutive response at each integration point of each element was described by the single crystal constitutive model through an ABAQUS UMAT subroutine [45]. The rigid model requires creating a new zone into the computational model, which cannot be realized by the conventional finite element due to its infinite stiffness and continuum formulation. The cohesive elements were thus employed to create new cracks. The incorporation of twinning has been proposed [46–49], and the predominant twin reorientation (PTR) scheme was utilized in the present study.

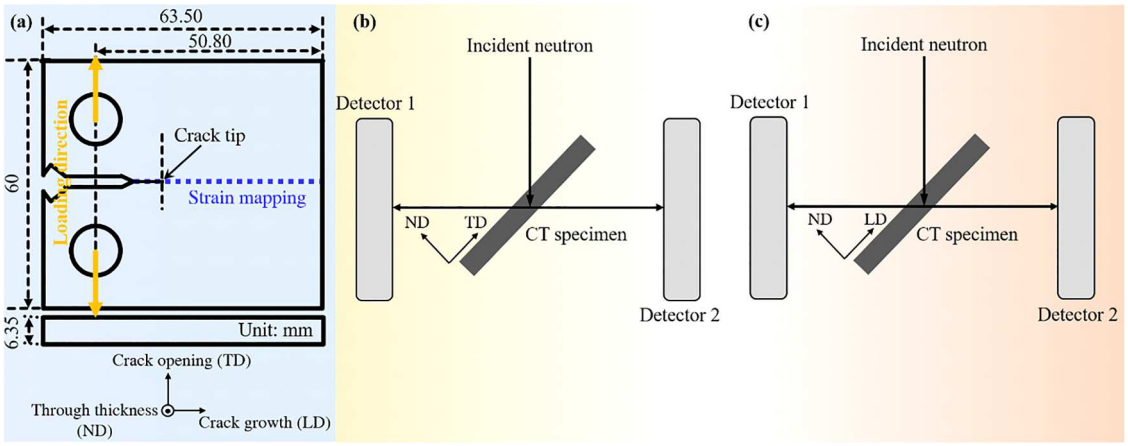

Fig. 1. (a) Schematic illustration of neutron-diffraction measurement arounds the crack tip of a CT specimen. (b) and (c) Neutron-diffraction geometry for the three-orthogonal strain mapping.

3. Results

3.1. Inhomogeneous chemical distribution

Fig. 2(a) and (b) show the POM observation of the as-fatigued and overloaded CoCrFeMnNi HEAs. Both the as-cast CoCrFeMnNi alloys revealed typical dendritic microstructures of dendrite and inter-dendrite regions. To explore the local distribution of each alloying element in these two different contrast regions, XRF maps with high spatial resolution were further employed, shown in Fig. 2(c) and (d). Both the CoCrFeMnNi HEAs under constant- and tensile-overloaded-fatigue conditions exhibited an inhomogeneous chemical distribution of constituent alloying compositions. The elemental segregation in the dendrite and inter-dendrite regions was visible in both alloys. The dendrite region was Co-Cr-Fe rich while the inter-dendrite region was Mn-Ni rich. Such a favorable distribution of Mn and Ni was ascribed to their lowest melting points and lowest mixing enthalpy in the binary system with respect to the other constituent elements [17,50–52]. Expectedly, immediately after a single tensile overload does not alter the elemental distribution in the CoCrFeMnNi dendritic microstructures under fatigue conditions.

3.2. Distribution of different crystallographic planes

To investigate the distribution of different crystallographic planes in the as-fatigued and overloaded CoCrFeMnNi HEAs, the evolution of neutron-diffraction intensities of various grain orientations as a function of the distance from the crack tip in the LD and TD directions was presented in Fig. 3. The typical crystallographic planes of {111}, {311}, and {422} orientations with less intergranular stresses in fcc materials were

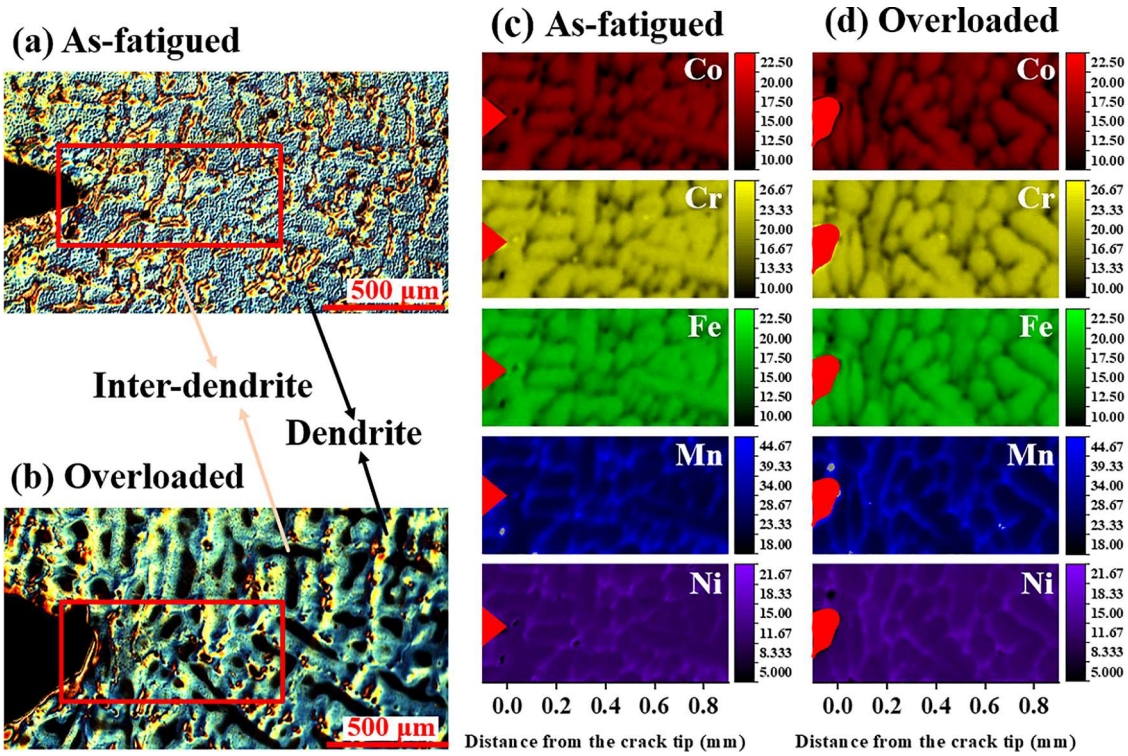

Fig. 2. POM micrographs of the (a) as-fatigued and (b) overloaded CoCrFeMnNi. (c) XRF maps of constituent alloying elements in the solid red square in (a); and (d) those in (b). (For interpretation of the references to colour in this figure legend, the reader is referred to the web version of this article.).

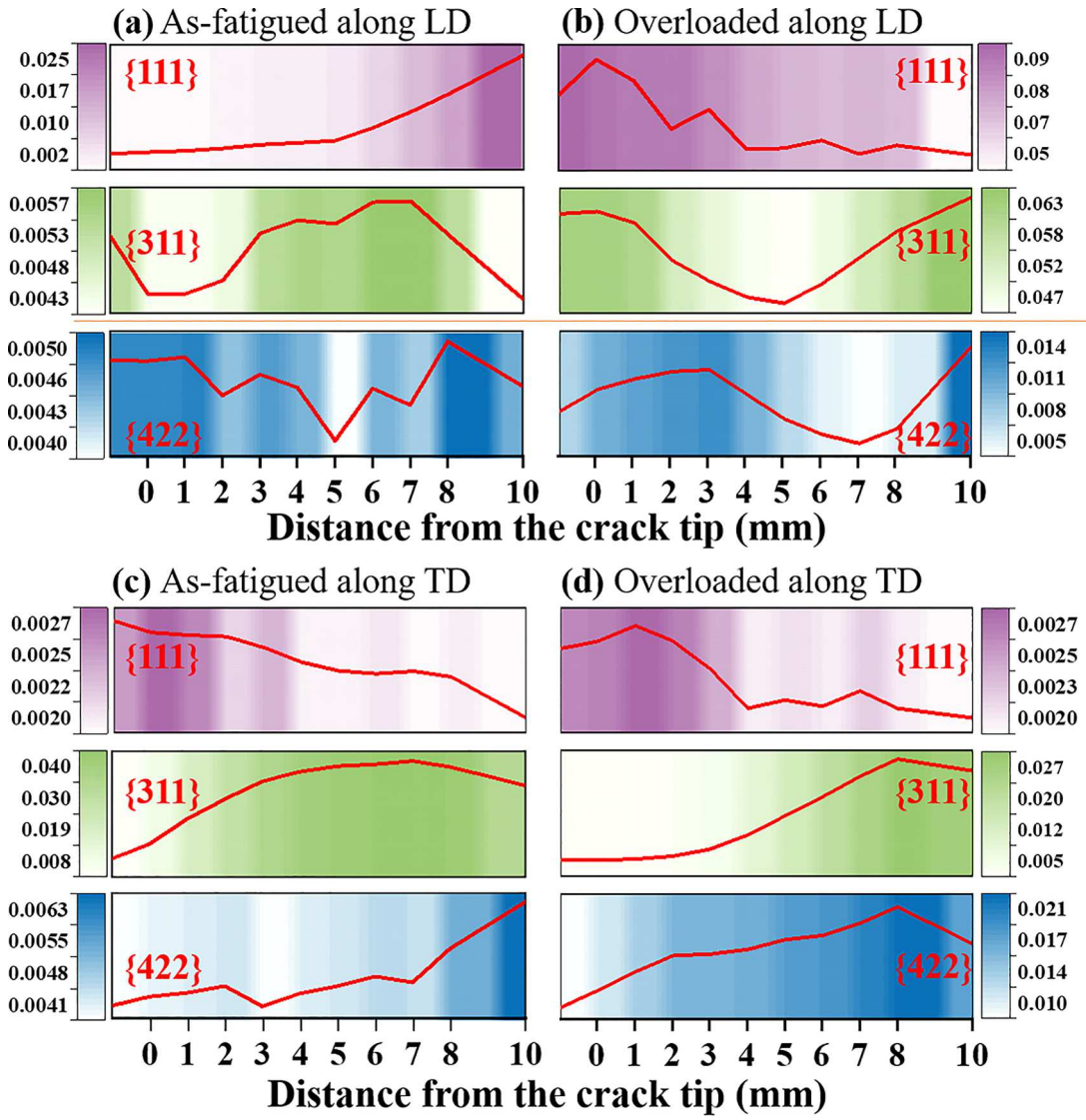

Fig. 3. Evolution of neutron-diffraction intensities of {111}, {311}, and {422} as a function of the distance from the crack tip in the (a) as-fatigued and (b) overloaded CoCrFeMnNi along the LD. Those in the (c) as-fatigued and (d) overloaded CoCrFeMnNi HEAs along the TD.

chosen [53]. The dominant distribution of {111} orientations under both fatigued conditions along the LD direction was identified in Fig. 3 (a) and (b). In Fig. 3(a), along the LD direction, among three distinct grain families, the {111} orientation displayed the most prominent increasing development ahead of the crack tip while a negligible evolution of the {311} and {422} orientations was seen. Immediately after a single tensile overload in Fig. 3(b), there was a similar decreasing evolution of the {111}, {311}, and {422} orientations within the plastic zone ahead of the crack tip.

Along the TD direction in Fig. 3(c) and (d), there was a similar propensity of each crystallographic plane with a considerably increasing evolution of the {311} orientation ahead of the crack tip under both fatigued conditions. There was a noticeably opposite tendency between {111} and {311}, {422} orientations in which a decreasing evolution of {111} orientation and a more pronounced increasing evolution of {311} and {422} orientations ahead of the crack tip were obtained under tensile overloaded-fatigue condition. Generally, the effects of immediately after a single tensile overload on the distribution of different crystallographic planes were negligible.

3.3. Crystallographic orientation under constant- and tensile-overloaded-fatigue conditions

Fig. 4(a) and (b) describe EBSD analysis with respect to the distance from the crack tip in the as-fatigued and overloaded CoCrFeMnNi HEAs. The EBSD results of grain-boundary distributions ahead of the crack tip suggested the energetically favorable transgranular crack propagation under both constant- and tensile-overloaded-fatigue conditions. Such a predominantly transgranular fracture was also observed in the FCP of the ultra-fine-grained CoCrFeMnNi HEA at room temperature [2]. Among distinct grain orientations, the (101)-oriented grains showed a more uniform structure since no evident substructures inside the (101)-oriented grains were seen in both HEAs. Meanwhile, the enlarged (111)-oriented grains in Fig. 4(e) indicated a more noticeable appearance of deformation twins in the overloaded sample rather than in the as-fatigued sample, which was in accordance with our previous results [10]. The presence of deformation twins along the crack path of transgranular fracture was also reported [54]. It is suggested that the (101)-oriented grains were least affected by plastic deformation ahead of the crack tip under both constant- and tensile-overloaded-fatigue conditions.

In Fig. 4(c), the grain surrounding the crack tip was divided into

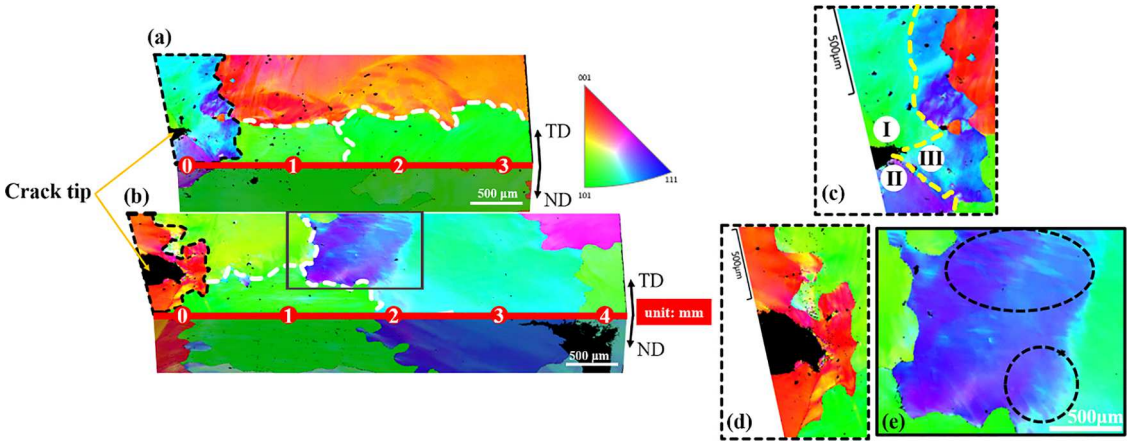

Fig. 4. EBSD analysis in the (a) as-fatigued and (b) overloaded CoCrFeMnNi. (c) The enlarged dotted black region in (a). (d) The enlarged dotted black region in (b). (e) The enlarged solid black region in (b). (For interpretation of the references to colour in this figure legend, the reader is referred to the web version of this article.).

three distinct oriented regions, which was presumably ascribed to the stress concentration at the tip of the pre-crack after stress unloading under a constant-fatigue condition. Such a phenomenon may facilitate the nucleation of a transgranular crack in the neighbouring grain for a steady crack propagation in a transgranular manner, which was discernible in the simulated stress contours, using a finite-element model [55]. However, a different orientation behavior surrounding the crack-tip blunting was distinguishable after stress unloading under a tensile-overloaded-fatigue condition. As observed in Fig. 4(d), the concentrated distribution of only the (001) orientation surrounding the crack-tip blunting was presumed to break the steady fatigue-crack growth and resist fatigue-crack propagation immediately after a single tensile overload. This feature is one of the possible reasons for the crack-growth-delay behavior in the overloaded CoCrFeMnNi HEA.

3.4. Crystal deformation under constant- and tensile-overloaded-fatigue conditions

Different deformation modes can be identified, using the full width at half maximum (FWHM) analysis of micro-X-ray diffraction mapping [56,57]. In the present study, we performed high spatial resolution XND mapping to understand the crack-tip deformation level ahead of the crack tip after stress unloading under constant- and tensile-overloaded-fatigue conditions. Fig. 5 presents the XND maps of the distribution of the full width of Laue diffraction with respect to the crack tip in both HEAs. The strongest deformation level was obtained at the crack tip due to the stress concentration at the tip of the fatigue crack after unloading under both fatigue conditions. However, their deformation behaviors were extremely different. In Fig. 5(a), the deformation was widely distributed ahead of the crack tip under a constant-fatigue condition. More visible paths with higher deformation levels nucleate the preferred propagating crack along the grain boundary (the dotted green line) or across the neighboring grains (the dotted red line) in the as-fatigued CoCrFeMnNi.

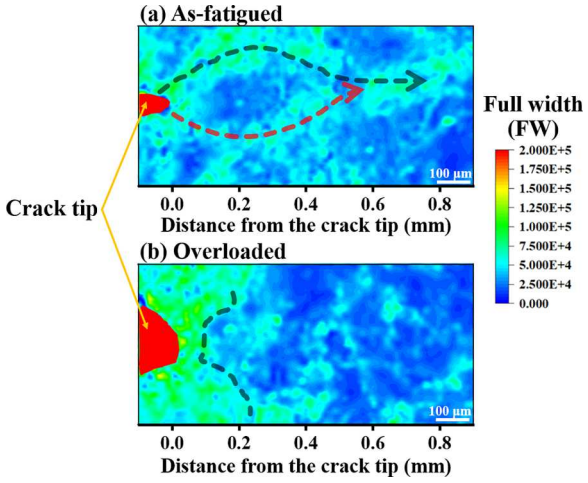

Fig. 5. XND maps with respect to the crack tip in the (a) as-fatigued and (b) overloaded CoCrFeMnNi HEAs.

In contrast to the as-fatigued sample, a much higher concentration of high deformation levels was confined, surrounding the crack-tip blunting in the overloaded sample, as shown in Fig. 5(b), which inhibits fatigue-crack growth immediately after a single tensile overload. Such a high energy barrier can be overcome by the fracture energy under further cyclic loading so that the transgranular crack enables to be across the adjacent grains and continue propagation. The XND results of the crack-tip blunting-induced high concentration of large deformation levels were in accordance with the EBSD analysis of the crack-tip blunting-induced concentrated distribution of grain orientations surrounding the crack tip, which is presumably responsible for retarding the crack-growth behavior in the CoCrFeMnNi HEA under a tensile-overloaded-fatigue condition.

3.5. Crystallographic textures under constant- and tensile-overloaded-fatigue conditions

The effects of predominated deformation texture components under constant- and tensile-overloaded-fatigue conditions were examined via the ODF analysis. Table 1 lists the appropriate deformation-texture components identified in the single-phase fcc CoCrFeMnNi HEA,

Table 1
Texture components in the CoCrFeMnNi HEA.

Texture component	Symbol	Euler angle (°) (φ_1, φ, φ_2)	Miller indices
G_R		90, 45, 0	{110}<110>
B_S		35, 45, 0	{110}<112>
G		0, 45, 0	{110}<001>
G/B		17, 45, 0	{110}<115>
Twinning		0/60, 55, 45	{111}<011>

including the representative symbols, the corresponding Euler angles, and Miller indices. The deformation-texture components observed under fatigue conditions consisted of the rotated-Goss (G_R, ◇, {110}<110>); Brass (B_S, ▲, {110}<112>); Goss (G, ◆, {110}<001>); G/B (●, {110}<115>), orientation lying between the G and B_S; and deformation twinning (✚, {111}<011>).

Fig. 6 presents the $\varphi_2 = 45^o$ section of the ODF evolution with respect to the distance from the crack tip along the crack-growth direction in the (a) as-fatigued and (b) overloaded CoCrFeMnNi HEAs. The ODF sections disclosed a main deformation texture of the G_R-type at the crack tip under a constant-fatigue condition. In accompanying with the G_R-type texture, an appearance of G/B and B_S-type textures was visible at the crack tip under a tensile-overloaded-fatigue condition. The deformation-texture components under both fatigue conditions varied with the propagating crack after stress unloading, and their texture-orientation behaviors were different as the crack propagated. Characterization of the ODF development indicated a gradual texture transition from the predominantly G_R-oriented to B_S-dominated region in the as-fatigued CoCrFeMnNi HEA. Meanwhile, there was a transition from a G_R-type texture to deformation twinning coupled with a Goss-type texture with the propagating crack and finally to a Goss-type texture as the crack continued to propagate in the overloaded CoCrFeMnNi HEA. The presence of a deformation-twinning texture under a tensile-overloaded-fatigue condition was in accordance with the single tensile-overload-induced deformation twinning, demonstrated in the overloaded CoCrFeMnNi HEA [10]. The twinning formation-driven shear deformation gave rise to the development of a Goss-type texture with the propagating crack in the overloaded sample.

The $\varphi_2 = 0^o$ section of the ODF evolution in Fig. 7 was also described to verify the deformation texture components-dominated fatigue-crack growth under fatigue conditions. The ODF development of the deformation-texture orientation at the $\varphi_2 = 0^o$ section was extremely analogous to that at the $\varphi_2 = 45^o$ section under a constant-fatigue condition. Specifically, a similar transition from a G_R to B_S orientation with the propagating crack in the as-fatigued CoCrFeMnNi HEA was obtained at the $\varphi_2 = 0^o$ section. Meanwhile, the dominant texture orientation in the overloaded CoCrFeMnNi HEA was originally from the G_R to G_R associated with G/B and B_S and finally to G coupled with G/B and B_S with the propagating crack. Examination of the ODF sections unveiled that the major difference in the deformation-texture orientation under constant-and tensile-overloaded-fatigue conditions was the remarkable Goss-type texture ahead of the crack tip immediately after a single tensile overload.

3.6. Twin-volume fraction around the crack tip simulated by CPEEM

To quantify the twin-volume fraction (TVF) distributed around the crack tip during FCP, CPEEM was performed under constant-and tensile-overloaded-fatigue conditions. The specimens were divided into 5810 elements with a 8-node hexahedral linear reduction integral element (C3D8), and the cohesive element was divided into 27 elements with eight junction three-dimensional bonding element (COH3D8). The geometric model was illustrated in Fig. 8(a). Fig. 8(b) presents the TVF as a function of the distance from the crack tip under both fatigue conditions. The TVF reached the highest value at the crack tip in both specimens. However, the overloaded CoCrFeMnNi disclosed a much greater TVF in the overload-induced enlarged plastic zone, compared to the as-fatigued specimen. The contour plots of TVF distributions around the crack tip were depicted in Fig. 8(c) and (d). The deformation twinning was distributed in a wider zone size with a dense concentration surrounding the crack tip in the overloaded specimen, totally in agreement with our previous results [10]. The CPEEM results strongly affirm the salient twinning structures-driven deformation behavior under a tensile-overloaded-fatigue condition in the CoCrFeMnNi.

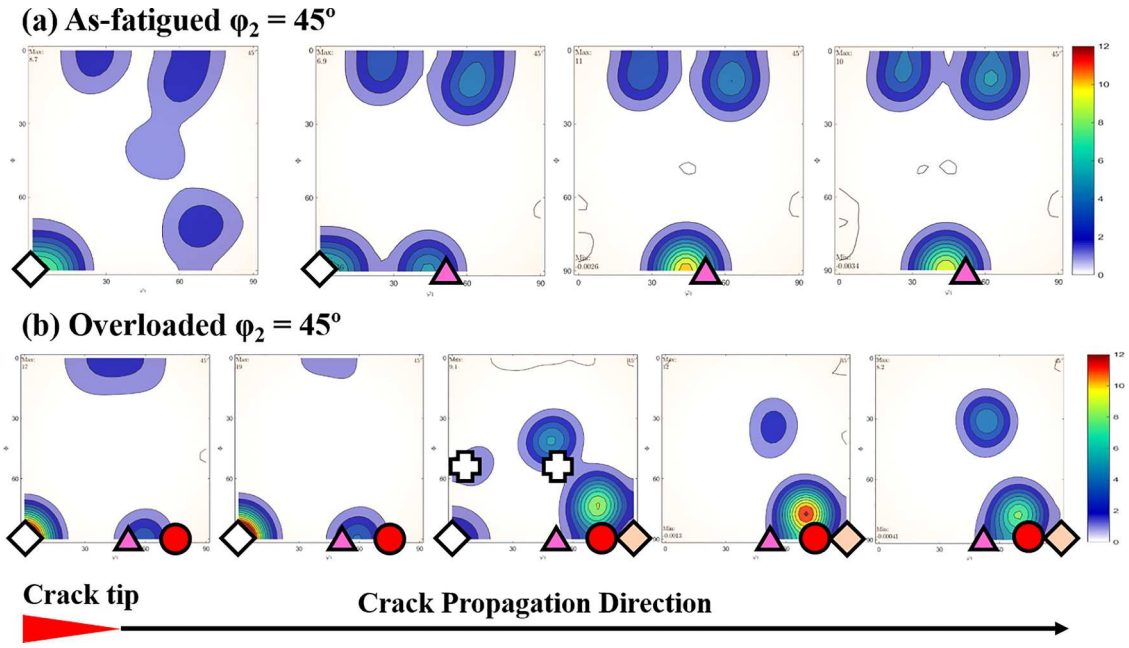

Fig. 6. $\varphi_2 = 45^o$ section of the ODF evolution with respect to the fatigue-crack propagation in the (a) as-fatigued and (b) overloaded CoCrFeMnNi HEAs. G_R, B_S, G, G/B, and deformation twinning were represented by ◇, ▲, ◆, ●, and ✚, respectively.

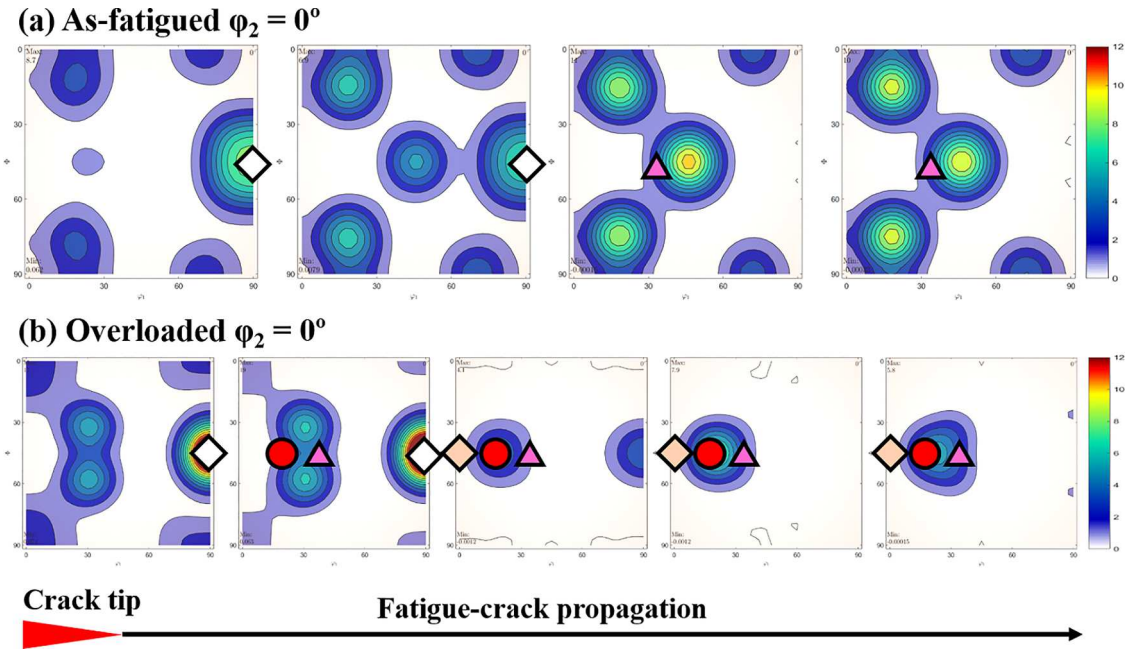

Fig. 7. $\varphi_2 = 0^o$ section of the ODF evolution with respect to the fatigue-crack propagation in the (a) as-fatigued and (b) overloaded CoCrFeMnNi HEAs. G_R, B_S, G, G/B, and deformation twinning were represented by ◇, △, ◈, ●, and ✚, respectively.

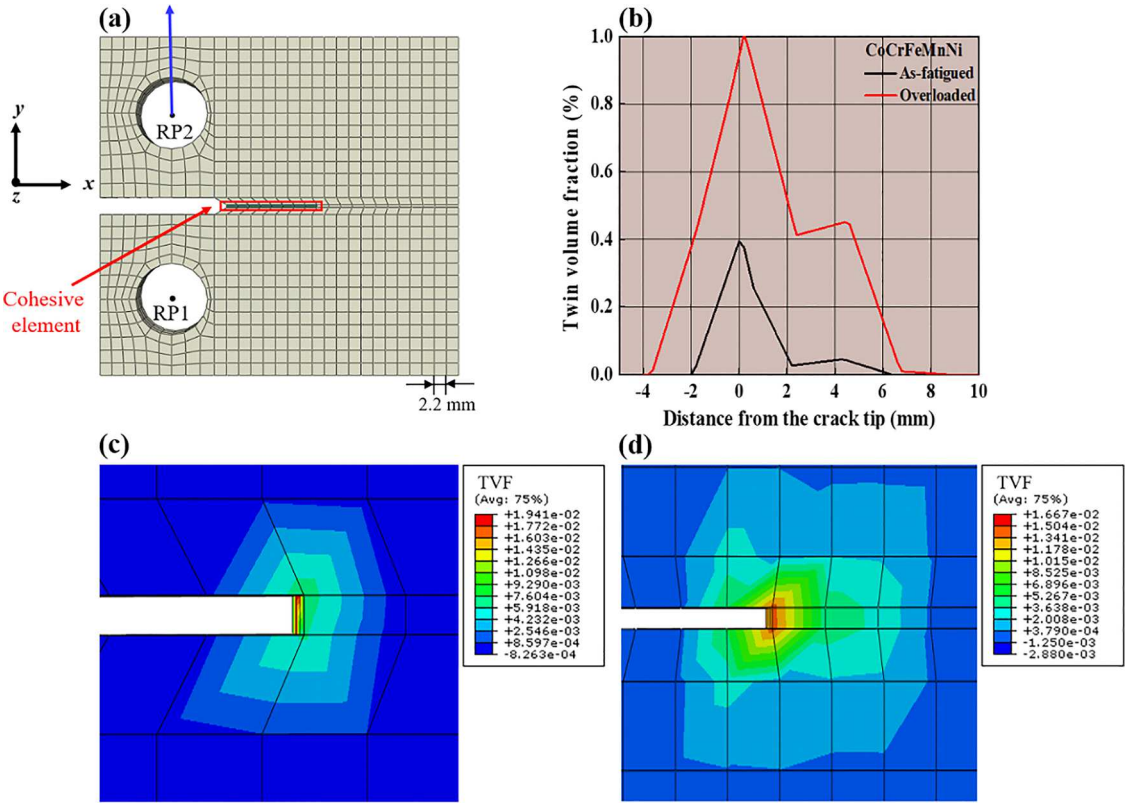

Fig. 8. (a) Geometric model of CPEEM simulation. (b) TVF distribution as a function of the distance from the crack tip in the as-fatigued and overloaded CoCrFeMnNi. The contour plots of TVF in the (c) as-fatigued and (d) overloaded CoCrFeMnNi HEAs.

4. Discussion

Understanding the relation among the grain size, grain orientation, and structural defect activities on the FCP under cyclic loading is significant to improve the fatigue resistance of the structural materials. The role of crack closure, such as grain size and dislocation or twinning activities, on the tensile-overload-induced crack-growth-retardation behavior in the coarse-grained CoCrFeMnNi was previously reported [10]. To gain a complete understanding of the tensile-overload-induced improved FCP resistance in the CoCrFeMnNi HEA, the influence of crack deflection occurring at the grain boundaries between various texture components was clarified.

After stress unloading under a constant-fatigue condition, the fatigue crack may propagate into neighboring grains along preferential slip systems in a widely uniform distribution of crystal- deformation levels, implying a steady crack propagation in the Paris regime, as demonstrated by the EBSD and XND results. However, the addition of a single tensile overload enabled to activate additional activities of deformation twinning, which induced a much larger deformation level surrounding the crack-tip blunting. When the fatigue crack approaches such a high energy barrier, the FCP rate significantly decreases. This trend results in the overload-induced crack-growth-retardation period in inhibiting the FCP resistance immediately after a single tensile-overload in the CoCrFeMnNi HEA.

The ODF evolution with respect to the crack tip indicated by the striking discrepancy of deformation texture components under constant- and tensile-overloaded-fatigue conditions was the formation of Goss orientation with the propagating crack within the plastic zone in the overloaded CoCrFeMnNi HEA. The development of the Brass-type texture under both fatigue conditions was mainly attributed to the induced plastic deformation in the low stacking-fault energy of the fcc CoCrFeMnNi HEAs [29,58–60]. Meanwhile, the formation of the Goss-type texture in the overloaded CoCrFeMnNi was presumably ascribed to the twinning formation-driven shear deformation. The deformation twining-coupled shear bands facilitated the development of a Goss texture in the heavily deformed CoCrFeMnNi under a tensile-overloaded-fatigue condition. Such a remarkable development of the Goss component was commonly obtained in the strongly deformed materials under cold rolling or recrystallization annealing [58,61,62]. Among the distinct texture components, the Goss-oriented grain was reported to own a large twist or great tilt angle boundary component with the neighboring grains [3,5]. Although the Brass-oriented grain also has a large tile angle with the neighboring grains, it is supposedly less resistant to FCP than the Goss-oriented grain [3,5,63]. The fatigue crack was prone to deflect more significantly when propagating across the grain boundary of a Goss orientation and thus led to great resistance to FCP [3,5,63,64]. The combined effects of the crack-tip blunting-induced concentrated orientation of (001) and high concentration of large deformation levels associated with the development of a Goss texture ahead of the crack tip delayed the overall fatigue-crack growth under a tensile-overloaded-fatigue condition in the Paris regime.

5. Conclusions

The effect of the grain orientation and texture on the tensile-overload-induced crack-growth-retardation behavior in the Paris regime within the dendritic microstructure of coarse-grained CoCrFeMnNi HEAs was extensively investigated. The crack-tip blunting-driven high deformation level concentrated around the crack tip inhibited fatigue-crack growth immediately after a single tensile overload. A transition from the G_R-predominant to B_S-predominant texture was found after stress unloading under a constant-fatigue condition. Meanwhile, an appreciable difference was the additional appearance of the Goss orientation with the propagating crack under a tensile-overloaded-fatigue condition. The twinning formation-driven shear deformation promoted the development of Goss-type texture within the overload-induced larger plastic deformation, which was believed to effectively resist the overall FCP performance. A complete understanding of tensile-overload-driven microstructure and texture effects on the enhanced resistance to FCP behavior is helpful in designing HEAs with better fatigue resistance under high-cycle fatigue.

Declaration of Competing Interest

The authors declare that they have no known competing financial interests or personal relationships that could have appeared to influence the work reported in this paper.

Acknowledgments

The neutron-diffraction experiments were performed at the BL19 in the Materials and Life Science Experimental Facility of J-PARC with the proposals of 2016A0322 and 2018A0248. We acknowledge the National Science and Technology Council (NSTC), Taiwan, for financial support through Grant No. MOST-108-2739-M-213-001 from the National Synchrotron Radiation Research Center (NSRRC) Neutron Cultivation Program, in providing the trip to J-PARC used in the present work. The authors are grateful to the support of the NSTC under Grant MOST 110-2224-E-007-001, MOST 108-2221-E-009-131-MY4, and MOST 111-2811-E-A49-503. We are very grateful to Prof. A.-C. Y. and Dr. Y.-J. C. for fabricating the high quality samples. This work was financially supported by the "High Entropy Materials Center" from The Featured Areas Research Center Program within the framework of the Higher Education Sprout Project by the Ministry of Education (MOE) and from the Project MOST 111-2634-F-007-008- by National Science and Technology Council (NSTC) in Taiwan. We really appreciate Prof. P. K. L. and Dr. R. F. for assisting the crack-growth experiment. This work was financially supported by the "Center for the Semiconductor Technology Research" from the Featured Areas Research Center Program within the framework of the Higher Education Sprout Project by the Ministry of Education (MOE) in Taiwan. Also supported in part by the National Science and Technology Council, Taiwan, under Grant No. NSTC 111-2634-F-A49-008-. SYL was supported by a National Research Foundation (NRF) grant funded by the Korean government (2021R1A4A1031494 and 2020R1I1A2070474). PKL is supported by the National Science Foundation (DMR-1611180, 1809640, and 2226508) and the US Army Research Office (W911NF-13-1-0438 and W911NF-19-2-0049).

References

[1] D.B. Miracle, O.N. Senkov, A critical review of high entropy alloys and related concepts, Acta Mater. 122 (2017) 448–511.
[2] K.V.S. Thurston, B. Gludovatz, A. Hohenwarter, G. Laplanche, E.P. George, R. O. Ritchie, Effect of temperature on the fatigue-crack growth behavior of the high-entropy alloy CrMnFeCoNi, Intermetallics 88 (2017) 65–72.
[3] Q. Zhao, Z. Liu, Y. Hu, F. Li, C. Luo, S. Li, Texture effect on fatigue crack propagation in aluminium alloys: an overview, Mater. Sci. Technol. 35 (15) (2019) 1789–1802.
[4] B. Künkler, O. Düber, P. Köster, U. Krupp, H.J. Christ, Modelling of short crack propagation – transition from stage I to stage II, Eng. Fract. Mech. 75 (3-4) (2008) 715–725.
[5] Z. Liu, F. Li, P. Xia, S. Bai, Y. Gu, D. Yu, S. Zeng, Mechanisms for Goss-grains induced crack deflection and enhanced fatigue crack propagation resistance in fatigue stage II of an AA2524 alloy, Mater. Sci. Eng. A 625 (2015) 271–277.
[6] R.L. Carlson, G.A. Kardomateas, P.R. Bates, The effects of overloads in fatigue crack growth, Int. J. Fatigue 13 (6) (1991) 453.
[7] S.Y. Lee, Y. Sun, K. An, H. Choo, C.R. Hubbard, P.K. Liaw, Evolution of residual-strain distribution through an overload-induced retardation period during fatigue-crack growth, J. Appl. Phys. 107 (2) (2010), 023517.
[8] S.Y. Lee, E.W. Huang, W. Woo, C. Yoon, H. Chae, S.G. Yoon, Dynamic strain evolution around a crack tip under steady- and overloaded-fatigue conditions, Metals 5 (4) (2015) 2109–2118.
[9] S. Seo, E.W. Huang, W. Woo, S.Y. Lee, Neutron diffraction residual stress analysis during fatigue crack growth retardation of stainless steel, Int. J. Fatigue 104 (2017) 408–415.
[10] T.N. Lam, S.Y. Lee, N.T. Tsou, H.S. Chou, B.H. Lai, Y.J. Chang, R. Feng, T. Kawasaki, S. Harjo, P.K. Liaw, A.C. Yeh, M.J. Li, R.F. Cai, S.C. Lo, E.W. Huang,

Enhancement of fatigue resistance by overload-induced deformation twinning in a CoCrFeMnNi high-entropy alloy, Acta Mater. 201 (2020) 412–424.
[11] C. Chen, D. Ye, L. Zhang, J. Liu, Effects of tensile/compressive overloads on fatigue crack growth behavior of an extra-low-interstitial titanium alloy, Int. J. Mech. Sci. 118 (2016) 55–66.
[12] C. Bathias, M. Vancon, Mechanisms of overload effect on fatigue crack propagation in aluminium alloys, Eng. Fract. Mech. 10 (2) (1978) 409–424.
[13] J.W. Yeh, S.K. Chen, S.J. Lin, J.Y. Gan, T.S. Chin, T.T. Shun, C.H. Tsau, S.Y. Chang, Nanostructured high-entropy alloys with multiple principal elements: Novel alloy design concepts and outcomes, Adv. Eng. Mater. 6 (5) (2004) 299–303.
[14] B. Gludovatz, A. Hohenwarter, D. Catoor, E.H. Chang, E.P. George, R.O. Ritchie, A fracture-resistant high-entropy alloy for cryogenic applications, Science 345 (6201) (2014) 1153–1158.
[15] M. Seifi, D. Li, Z. Yong, P.K. Liaw, J.J. Lewandowski, Fracture toughness and fatigue crack growth behavior of as-cast high-entropy alloys, JOM 67 (10) (2015) 2288–2295.
[16] Z. Zhang, M.M. Mao, J. Wang, B. Gludovatz, Z. Zhang, S.X. Mao, E.P. George, Q. Yu, R.O. Ritchie, Nanoscale origins of the damage tolerance of the high-entropy alloy CrMnFeCoNi, Nat. Commun. 6 (10143) (2015) 1–6.
[17] B. Cantor, I.T.H. Chang, P. Knight, A.J.B. Vincent, Microstructural development in equiatomic multicomponent alloys, Mater. Sci. Eng. A 375-377 (2004) 213–218.
[18] E.W. Huang, G.Y. Hung, S.Y. Lee, J. Jain, K.P. Chang, J.J. Chou, W.C. Yang, P. K. Liaw, Mechanical and magnetic properties of the high-entropy alloys for combinatorial approaches, Crystals 10 (3) (2020) 200.
[19] E.W. Huang, W.J. Lee, S.S. Singh, P. Kumar, C.Y. Lee, T.N. Lam, H.H. Chin, B. H. Lin, P.K. Liaw, Machine-learning and high-throughput studies for high-entropy materials, Mater. Sci. Eng. R Rep. 147 (2022), 100645.
[20] M.Y. Luo, T.N. Lam, P.T. Wang, N.T. Tsou, Y.J. Chang, R. Feng, T. Kawasaki, S. Harjo, P.K. Liaw, A.C. Yeh, S.Y. Lee, J. Jain, E.W. Huang, Grain-size-dependent microstructure effects on cyclic deformation mechanisms in CoCrFeMnNi high-entropy-alloys, Scr. Mater. 210 (2022), 114459.
[21] T.N. Lam, C.W. Tsai, B.K. Chen, B.H. Lai, H.C. Liu, T. Kawasaki, S. Harjo, B.H. Lin, E.W. Huang, Element effects of Mn and Ge on the tuning of mechanical properties of high-entropy alloys, Metall. Mater. Trans. A 51 (10) (2020) 5023–5028.
[22] E.W. Huang, H.S. Chou, K.N. Tu, W.S. Hung, T.N. Lam, C.W. Tsai, C.Y. Chiang, B. H. Lin, A.C. Yeh, S.H. Chang, Y.J. Chang, J.J. Yang, X.Y. Li, C.S. Ku, K. An, Y. W. Chang, Y.L. Jao, Element effects on high-entropy alloy vacancy and heterogeneous lattice distortion subjected to quasi-equilibrium heating, Sci. Rep. 9 (1) (2019) 14788.
[23] W. Li, D. Xie, D. Li, Y. Zhang, Y. Gao, P.K. Liaw, Mechanical behavior of high-entropy alloys, Prog. Mater. Sci. 118 (2021), 100777.
[24] K.H. Lin, S.Y. Chang, Y.C. Lo, C.C. Wang, S.J. Lin, J.W. Yeh, Differences in texture evolution from low-entropy to high-entropy face-centered cubic alloys during tension test, Intermetallics 118 (2020), 106635.
[25] Z. Tang, T. Yuan, C.W. Tsai, J.W. Yeh, C.D. Lundin, P.K. Liaw, Fatigue behavior of a wrought Al0.5CoCrCuFeNi two-phase high-entropy alloy, Acta Mater. 99 (2015) 247–258.
[26] M.A. Hemphill, T. Yuan, G.Y. Wang, J.W. Yeh, C.W. Tsai, A. Chuang, P.K. Liaw, Fatigue behavior of Al0.5CoCrCuFeNi high entropy alloys, Acta Mater. 60 (16) (2012) 5723–5734.
[27] J. Rackwitz, Q. Yu, Y. Yang, G. Laplanche, E.P. George, A.M. Minor, R.O. Ritchie, Effects of cryogenic temperature and grain size on fatigue-crack propagation in the medium-entropy CrCoNi alloy, Acta Mater. 200 (2020) 351–365.
[28] K.V.S. Thurston, B. Gludovatz, Q. Yu, G. Laplanche, E.P. George, R.O. Ritchie, Temperature and load-ratio dependent fatigue-crack growth in the CrMnFeCoNi high-entropy alloy, J. Alloy. Compd. 794 (2019) 525–533.
[29] P.P. Bhattacharjee, G.D. Sathiaraj, M. Zaid, J.R. Gatti, C. Lee, C.W. Tsai, J.W. Yeh, Microstructure and texture evolution during annealing of equiatomic CoCrFeMnNi high-entropy alloy, J. Alloy. Compd. 587 (2014) 544–552.
[30] J. Saha, R. Saha, P.P. Bhattacharjee, Microstructure and texture development in CoCrNi medium entropy alloy processed by severe warm cross-rolling and annealing, Intermetallics 143 (2022), 107463.
[31] I.S. Wani, G.D. Sathiaraj, M.Z. Ahmed, S.R. Reddy, P.P. Bhattacharjee, Evolution of microstructure and texture during thermo-mechanical processing of a two phase Al0.5CoCrFeMnNi high entropy alloy, Mater. Charact. 118 (2016) 417–424.
[32] American Society for Testing and Materials (ASTM). Standard test method for measurement of fatigue crack-growth rates; ASTM Standard E647-99, American Society for Testing and, Materials: West Conshohocken, PA, USA, 2000, pp. 591–630.
[33] F. Bachmann, R. Hielscher, H. Schaeben, Texture analysis with MTEX – free and open source software toolbox, Solid State Phenom. 160 (2010) 63–68.
[34] C. Merola, H.W. Cheng, D. Dworschak, C.S. Ku, C.Y. Chiang, F.U. Renner, M. Valtiner, Nanometer resolved real time visualization of acidification and material breakdown in confinement, Adv. Mater. Interfaces 6 (10) (2019), 1802069.
[35] Abaqus, Users' Manual, Version 6.7, ABAQUS, Inc, 2008.
[36] R.J. Asaro, J.R. Rice, Strain localization in ductile single crystals, J. Mech. Phys. Solids 25 (5) (1977) 309–338.
[37] R.J. Asaro, Crystal plasticity, J. Appl. Mech. 50 (1983) 921–934.
[38] R.J. Asaro, Micromechanics of crystals and polycrystals, Adv. Appl. Mech. 23 (1983) 1–115.
[39] R.J. Asaro, A. Needleman, Texture development and strain hardening in rate dependent polycrystals, Acta Metall. 33 (1985) 923–953.
[40] R. Hill, Generalized constitutive relations for incremental deformation of metal crystals by multislip, J. Mech. Phys. Solid 14 (2) (1966) 95–102.
[41] Y. Huang, A user-material subroutine incorporating single crystal plasticity in the ABAQUS finite element program. Mech Report 178, Division of Engineering and Applied Sciences, Harvard University, 1991.
[42] D. Peirce, R.J. Asaro, A. Needleman, An analysis of nonuniform and localized deformation in ductile single crystals, Acta Metall. 30 (6) (1982) 1087–1119.
[43] D. Peirce, R.J. Asaro, A. Needleman, Material rate dependence and localized deformation in crystalline solids, Acta Metall. 31 (12) (1983) 1951–1976.
[44] J.R. Rice, Inelastic constitutive relations for solids: an internal-variable theory and its application to metal plasticity, J. Mech. Phys. Solids 19 (6) (1971) 433–455.
[45] H. Qiao, M.R. Barnett, P.D. Wu, Modeling of twin formation, propagation and growth in a Mg single crystal based on crystal plasticity finite element method, Int. J. Plast. 86 (2016) 70–92.
[46] C.N. Tomé, R.A. Lebensohn, U.F. Kocks, A model for texture development dominated by deformation twinning: Application to zirconium alloys, Acta Metall. Mater. 39 (11) (1991) 2667–2680.
[47] P.V. Houtte, Simulation of the rolling and shear texture of brass by the Taylor theory adapted for mechanical twinning, Acta Metall. 26 (4) (1978) 591–604.
[48] H. Wang, P.D. Wu, C.N. Tomé, J. Wang, A constitutive model of twinning and detwinning for hexagonal close packed polycrystals, Mater. Sci. Eng. A 555 (2012) 93–98.
[49] H. Wang, P.D. Wu, J. Wang, C.N. Tomé, A crystal plasticity model for hexagonal close packed (HCP) crystals including twinning and de-twinning mechanisms, Int. J. Plast. 49 (2013) 36–52.
[50] M. Laurent-Brocq, A. Akhatova, L. Perrière, S. Chebini, X. Sauvage, E. Leroy, Y. Champion, Insights into the phase diagram of the CrMnFeCoNi high entropy alloy, Acta Mater. 88 (2015) 355–365.
[51] T. Nagase, M. Todai, T. Nakano, Liquid phase separation in Ag-Co-Cr-Fe-Mn-Ni, Co Cr-Cu-Fe-Mn-Ni and Co-Cr-Cu-Fe-Mn-Ni-B high entropy alloys for biomedical application, Crystals 10 (6) (2020) 527.
[52] G.A. Salishchev, M.A. Tikhonovsky, D.G. Shaysultanov, N.D. Stepanov, A. V. Kuznetsov, I.V. Kolodiy, A.S. Tortika, O.N. Senkov, Effect of Mn and V on structure and mechanical properties of high-entropy alloys based on CoCrFeNi system, J. Alloy. Compd. 591 (2014) 11–21.
[53] M.T. Hutchings, P.J. Withers, T.M. Holden, T. Lorentzen. Introduction to the characterization of residual stress by neutron diffraction, CRC Press, Taylor & Francis, New York, 2005.
[54] Q. Xie, Z. Yan, D. Yu, K. An, X. Yan, S. Yin, B. Gillham, X. Wu, P. Yang, Z. Zhao, Y. Wang, Crystallographic orientation and spatially resolved damage for polycrystalline deformation of a high manganese steel, Acta Mater. 226 (2022), 117628.
[55] R.H. Kraft, J.F. Molinari, A statistical investigation of the effects of grain boundary properties on transgranular fracture, Acta Mater. 56 (17) (2008) 4739–4749.
[56] R. Li, Q. Xie, Y.D. Wang, W. Liu, M. Wang, G. Wu, X. Li, M. Zhang, Z. Lu, C. Geng, T. Zhu, Unraveling submicron-scale mechanical heterogeneity by three-dimensional X-ray microdiffraction, PNAS 115 (3) (2018) 483–488.
[57] R. Feng, Y. Rao, C. Liu, X. Xie, D. Yu, Y. Chen, M. Ghazisaeidi, T. Ungar, H. Wang, K. An, P.K. Liaw, Enhancing fatigue life by ductile-transformable multicomponent B2 precipitates in a high-entropy alloy, Nat. Commun. 12 (3588) (2021) 1–10.
[58] B.C.D. Cooman, Phase transformations in high manganese twinning-induced plasticity (TWIP) steels, in: Phase Transformations in Steels; Diffusionless Transformations, High Strength Steels, Modelling and Advanced Analytical Techniques, Volume 2, Woodhead publishing series in Metals and Surface Engineering, 2012, pp. 295–331.
[59] S. Picak, T. Wegener, S.V. Sajadifar, C. Sobrero, J. Richter, H. Kim, T. Niendorf, I. Karaman, On the low-cycle fatigue response of CoCrNiFeMn high entropy alloy with ultra-fine grain structure, Acta Mater. 205 (2021), 116540.
[60] T. Leffers, R.K. Ray, The brass-type texture and its deviation from the copper-type texture, Prog. Mater. Sci. 54 (3) (2009) 351–396.
[61] I. Kim, S.K. Nam, G.H. Kim, D.N. Lee, Goss Texture Formation by Asymmetric Rolling in Steel Sheet, Mater. Sci. Forum 917 (2018) 236–240.
[62] R.Y. Liang, P. Yang, W.M. Mao, Effect of initial Goss texture sharpness on texture evolution and magnetic properties of ultra-thin grain-oriented electrical steel, Acta Metall. Sin. Engl. Lett. 30 (9) (2017) 895–906.
[63] T. Zhai, X.P. Jiang, J.X. Li, M.D. Garratt, G.H. Bray, The grain boundary geometry for optimum resistance to growth of short fatigue cracks in high strength Al-alloys, Int. J. Fatigue 27 (10-12) (2005) 1202–1209.
[64] F. Li, Z. Liu, W. Wu, P. Xia, P. Ying, Y. Zhou, W. Liu, L. Lu, A. Wang, Enhanced fatigue crack propagation resistance of Al-Cu-Mg alloy by intensifying Goss texture and refining goss grains, Mater. Sci. Eng. A 679 (2017) 204–214.